Consideration of Rotational Motion in the Proper Generalized Decomposition by a Sliding Interface Technique

Fabian Müller and Kay Hameyer

Institute of Electrical Machines (IEM), RWTH Aachen University, 52062 Aachen, Germany

The simulation of rotating electrical machines, particularly in the development process, involves many parameters, such as the current excitation, permanent magnet materials, and the relative rotor position. To reduce the computational effort related to a large number of degrees of freedom (DOFs), the proper generalized decomposition (PGD) can be employed. Although the mentioned reduction technique is able to efficiently cope with parameter variations, it is limited to conformal meshes. However, the consideration of moving parts in the model for the simulation of rotating electrical machines is a necessity to characterize the machine's behavior. For this purpose, the sliding interface technique, based on Lagrange multipliers (LMs) can be utilized. In this contribution, the sliding interface technique, which imposes no restrictions on the finite element discretization of the interface between stator and rotor, is combined with the PGD to lift the restriction of the latter to conformal meshes while keeping the symmetry and positive definiteness of the system without the creation of additional elements. This approach enables the parametric simulation of rotating electrical machines by the PGD.

Index Terms—**Lagrange multiplier (LM), model order reduction (MOR), motion, proper generalized decomposition (PGD), sliding interfaces.**

I. Introduction

In THE simulation of electrical machines, a restriction to conformally meshed geometries represents an undesired condition because in most rotating electrical machines motion has to be considered. While, in standard finite element simulation, this limitation is coped with by techniques such as overlapping elements [1], the moving-band method [2], the mortar element method [3], [4], or sliding interfaces [5], it is still challenging if the proper generalized decomposition (PGD) is used. The PGD, as an *a priori* model order reduction (MOR) technique, can show large reduction of computational effort [6] and is already applied to a variety of electromagnetic field problems [6]–[9]. The PGD is applicable to separable problems, but the consideration of motion states a non-separable problem. This non-separability is associated with modification in the system due to motion-related changes of the connection between degrees of freedom (DOFs) on the interface. In [7], an approach based on the overlapping element method is presented to consider motion in the PGD. The overlapping element method is based on creating additional elements in the overlapping region without introducing new DOF [1]. In this contribution, an approach considering a motion by a non-conforming sliding interface is employed without the necessity to construct additional elements for each angular position. The Lagrange multipliers (LMs) utilized in this technique can be efficiently used to couple the static and moving domains [10], [11] and keep the positive symmetric semi-definite property of the system. This combination of the sliding interface technique and the PGD rotating electrical machines can be studied.

Manuscript received 8 February 2022; revised 6 March 2022; accepted 8 March 2022. Date of publication 14 March 2022; date of current version 26 August 2022. Corresponding author: F. Müller (e-mail: fabian.mueller@iem.rwth-aachen.de).

Color versions of one or more figures in this article are available at https://doi.org/10.1109/TMAG.2022.3159093.

Digital Object Identifier 10.1109/TMAG.2022.3159093

II. Finite Element Formulation

To solve electromagnetic fields in electrical machines, neglecting eddy currents, the static magnetic vector potential formulation is widely applied. A geometry shall be decomposed into two domains, the slave domain Ω^{S} and the master domain Ω^{M}, and both domains are not connected. The boundaries of the domains are denoted as Γ^{S}, Γ^{M} and $\Gamma^{\mathrm{D}} = \partial\Omega^{\mathrm{M}} \setminus \Gamma^{\mathrm{M}} \cup \partial\Omega^{\mathrm{S}} \setminus \Gamma^{\mathrm{S}}$. While Γ^{S} and Γ^{M} form the interface between Ω^{S} and Ω^{M}, Γ^{D} holds unary boundary conditions. In addition, a mapping between Γ^{S} and Γ^{M} is given by $p : \Gamma^{\mathrm{M}} \rightarrow \Gamma^{\mathrm{s}}$, and the master potential is then mapped to the slave curvature by $A^{\mathrm{M}} \circ p$. Introducing these boundaries into the vector potential formulation results in the following equation [5]:

$$\begin{aligned}\sum_{k=\mathrm{M,S}} \int_{\Omega^k} \nu\nabla\times\boldsymbol{A}\nabla\times\alpha + \nu\boldsymbol{B}_{\mathrm{PM}}\nabla\times\alpha + \boldsymbol{J}\alpha d\Omega^k \\ + \int_{\Gamma^{\mathrm{S}}} \left(\lambda^{\mathrm{S}} - \boldsymbol{H}^{\mathrm{S}}\times n^{\mathrm{S}}\right)\alpha^{\mathrm{S}} d\Gamma^{\mathrm{S}} \\ - \int_{\Gamma^{\mathrm{M}}} \left(\lambda\circ p^{-1} + \boldsymbol{H}^{\mathrm{M}}\times n^{\mathrm{M}}\right)\alpha^{\mathrm{M}} d\Gamma^{\mathrm{M}} \\ + \int_{\Gamma^{\mathrm{S}}} \mu\left(\boldsymbol{A}^{\mathrm{S}} - \boldsymbol{A}^{\mathrm{M}}\circ p\right) d\Gamma^{\mathrm{S}} = 0. \end{aligned} \tag{1}$$

$\boldsymbol{A}$ is the magnetic vector potential, and α denotes the nodal form function, employed as test and weighting function accordingly to the Galerkins method. $\boldsymbol{J}$ is the current, and $\boldsymbol{B}_{\mathrm{PM}}$ is the excitation given by permanent magnets. λ denotes the LM, a penalty term to ensure continuity over the interface, and μ denotes the form function associated with the LM on the interface. The three curvature integrals in (1) ensure the continuity of the magnetic field strength and the vector potential over the interface. In [5] and [10], a more in-depth explanation is given. To keep the positive semi-definite property of conformal problems, it is possible to transform the saddle point problem resulting from (1) into a symmetric form.

0018-9464 © 2022 IEEE. Personal use is permitted, but republication/redistribution requires IEEE permission.
See https://www.ieee.org/publications/rights/index.html for more information.

Authorized licensed use limited to: Universitaetsbibliothek der RWTH Aachen. Downloaded on November 04,2022 at 11:31:00 UTC from IEEE Xplore. Restrictions apply.

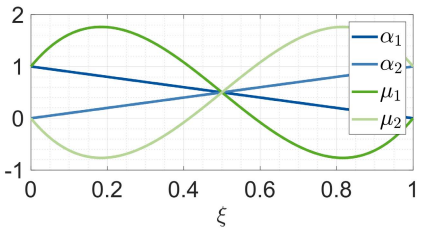

Fig. 1. First-order nodal form functions.

For this purpose, the LM and the related DOF are eliminated by imposing additional boundary constraints. The constraints are computed by

$$\boldsymbol{A}^{\mathrm{S}} = \left(\int_{\Gamma^{\mathrm{S}}} \mu\alpha^{\mathrm{S}} d\Gamma^{\mathrm{S}}\right)^{-1} \int_{\Gamma^{\mathrm{S}}} \mu\alpha^{\mathrm{M}} \circ p d\Gamma^{\mathrm{S}} \boldsymbol{A}^{\mathrm{M}}. \tag{2}$$

To efficiently compute the additional boundary constraints, it is necessary to employ biorthogonal form functions for μ, which simplifies the computation of the inverse in (2) [5], [11]

$$\int_{\Gamma^{\mathrm{S}}} \mu_i \alpha_j^{\mathrm{S}} d\Gamma^{\mathrm{S}} = \delta_{ij} \int_{\Gamma^{\mathrm{S}}} \alpha_j^{\mathrm{S}} d\Gamma^{\mathrm{S}}, \quad \text{with} \quad \delta_{ij} = \begin{cases} 1, & \text{if } i = j \\ 0, & \text{if } i \neq j. \end{cases} \tag{3}$$

The nodal form functions and continuous biorthogonal form functions for a first-order line element are given in Fig. 1.

III. PGD With Motion

The PGD separates the unknown potential into a sum over products of functions, which only depends on one parameter, such as $\boldsymbol{R}(x)$ for the space and $T_i(\theta)$ for the motion (4). The test function $\alpha = \partial A$, due to the Galerkins method, is derived by (5)

$$\begin{aligned} &\boldsymbol{A}(x, \theta, p_1, \ldots, p_n) \\ &\quad = \sum_{i=1}^{m} \boldsymbol{R}_i(x) \cdot T_i(\theta) \cdot F_{1,i}(p_1) \cdots F_{n,i}(p_n) \qquad (4) \\ &\alpha = \boldsymbol{R}'_m(x) \cdot T_m(\theta) \cdot F_{1,m}(p_1) \cdots F_n(p_n) + \cdots \\ &\quad + \boldsymbol{R}_m(x) \cdot T_m(\theta) \cdot F_{1,m}(p_1) \cdots F'_n(p_n). \qquad (5) \end{aligned}$$

The parameter θ denotes the rotor angle, and p_1 to p_n can be chosen, for example, as the permanent magnet remanence, the current amplitude, or other problem-related parameters. In the first step, (4) and (5) are introduced into (1), and consecutively, the formulation is rearranged according to the parameter integration. Employing an alternative direction scheme (ADS) enables to sequentially solve for the different parameters [9]. The subscript depicts the mode number in the following explanations, and to simplify the equations, the PGD will only contain the angle function $F(\theta)$ and the spatial component R, while the permanent magnet remanence is kept constant. The current is a function of θ as well. Nevertheless, the procedure is similar if more parameters are introduced. Nonlinearities are considered by employing a fixed-point reluctivity ν_{fp} and a magnetization term $\boldsymbol{H}_{\mathrm{fp}}$ in combination with the discrete empirical interpolation method (DEIM) [9], [12]. This approach is mainly employed in separable problems [8], [9], which is not given if motion shall be included. The relative position of the domains affects the connection of the DOF on the interface (2) and, therefore, changes the system matrix. Due to this reason, the problem is subdivided into a decomposable part and a non-decomposable part similar to [7]. In the following, the enriched model is referred to as reduced-order model (ROM).

A. Space Computation

The evaluation of the spatial component introduces an additional splitting of the stationary and rotating domains into a part $\Omega^{k,\mathrm{int}}$ and $\Omega^{k,\mathrm{air}}$. The first one consists of all elements not connected to the interface and has an underlying piecewise affine decomposition (PAD), while the latter one consists of elements in the airgap, which are connected to either Γ^m or Γ^s, which has no underlying PAD [5], [7]. The domain $\Omega^{k,\mathrm{int}}$ can be treated as in [6], [8], and [9]. By assuming that the modes up to $m-1$ are known, then the system of the separable regions is given by the following equation:

$$\begin{aligned} &\sum_{k=\mathrm{M,S}} \int_{\Omega^{\mathrm{k,int}}} \nu_{\mathrm{fp}} \nabla \times \boldsymbol{R}_m \nabla \times \boldsymbol{R}'_m d\Omega^{\mathrm{k,int}} \int_{\Theta} (T_m(\theta))^2 d\theta \\ &= \sum_{k=\mathrm{M,S}} \int_{\Omega^{\mathrm{k,int}}} \boldsymbol{J}_x \boldsymbol{R}'_m d\Omega^{\mathrm{k,int}} \int_{\Theta} J_\theta T_m(\theta) d\theta \\ &\quad + \sum_{k=\mathrm{M,S}} \int_{\Omega^{\mathrm{k,int}}} \nu B_{\mathrm{PM},x} \nabla \times \boldsymbol{R}'_m d\Omega^{\mathrm{k,int}} \int_{\Theta} B_{\mathrm{PM},\theta} T_m(\theta) d\theta \\ &\quad - \sum_{i=1}^{m-1} \nu_{\mathrm{fp}} \nabla \times \boldsymbol{R}_i \nabla \times \boldsymbol{R}'_m d\Omega^{\mathrm{k,int}} \int_{\Theta} T_i(\theta) T_m(\theta) d\theta \\ &\quad - \sum_{k=\mathrm{M,S}} \int_{\Theta} T_m(\theta) \int_{\Omega^{\mathrm{k,int}}} \left(\nabla \times \boldsymbol{H}_{\mathrm{fp}}(\boldsymbol{A}(x,\theta)) \boldsymbol{R}'_m d\Omega^{\mathrm{k,int}} d\theta\right). \end{aligned} \tag{6}$$

The airgap region Ω^{air} needs to consider the connection between the slave and master domains, including a projection operator p, which depends on the relative rotor position, and due to this reason, the submatrix unavoidably has to be rebuilt for each angle θ_l. A weighted sum is used to build an approximation of the matrix in Ω^{air} over all positions, including the integration over all parameters except for θ, which is then added to the matrix of $\Omega^{k,\mathrm{int}}$ [7]. Furthermore, to completely extract the information content of previous modes from the equation system, the non-separable part has to be considered on the right-hand side. For this purpose, the matrix in Ω_{air} is built and multiplied with the space modes up to $m-1$. The resulting system of equations (7) can be solved by standard Krylov-subspace algorithms, such as the conjugate gradient method

$$\begin{aligned} &\left(\sum_{\mathrm{k=m,s}} \mathbf{M}_{k,\mathrm{int}} + \sum_{l} \mathbf{M}_{\mathrm{air}}(\theta_l)\right) \boldsymbol{R}_m \\ &\qquad = B - \sum_{i=1}^{m-1} \sum_{l} \mathbf{M}_{\mathrm{air}}(\theta_l) T_i(\theta_l) T_m(\theta_l) \boldsymbol{R}_i d\theta. \end{aligned} \tag{7}$$

B. Angular Computation

To evaluate the angular mode, the spatial component $\boldsymbol{R}_m$ is assumed to be known from the previous computation (6), (7);

Authorized licensed use limited to: Universitaetsbibliothek der RWTH Aachen. Downloaded on November 04,2022 at 11:31:00 UTC from IEEE Xplore. Restrictions apply.

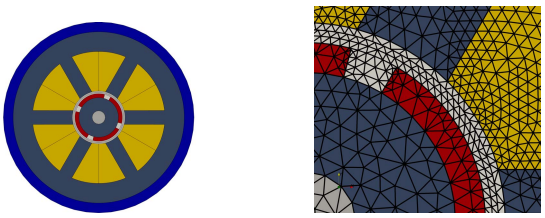

(a) (b)

Fig. 2. Studied permanent magnet synchronous machine. (a) Problem geometries. (b) Non-conform mesh in the airgap.

hence, it is possible to evaluate the integrals in Ω_k, leading to a linear equation to be solved for all rotational positions. The term H_{NL} belongs to the non-linearity, while H_{Lin} extracts the information of the modes up to $m-1$. To evaluate the curl of the vector potential, it is necessary to apply the projection operator on beforehand, denoted by the function F, which maps the potential of the master nodes back onto the slave curvature. Several nodes on the master interface are connected to one slave node by a factor $\kappa_j(\theta)$

$$A_{\mathrm{move}} \cdot T(\theta) + L(\theta) = C_{\mathrm{move}} \cdot J(\theta) + D_{\mathrm{move}} - L_d(\theta) - H_{\mathrm{Lin}}(\theta) - H_{\mathrm{NL}}(\theta) \tag{8}$$

$$A_{\mathrm{move}} = \sum_{k=\mathrm{M,S}} \int_{\Omega^{k,\mathrm{int}}} \nabla \times R_m^k \nabla \times R_m^k d\Omega^{k,\mathrm{int}} \tag{9}$$

$$C_{\mathrm{move}} = \sum_{k=\mathrm{M,S}} \int_{\Omega^{k,\mathrm{int}}} J_{\mathrm{x}} \boldsymbol{R}_m^k d\Omega^{k,\mathrm{int}} \tag{10}$$

$$D_{\mathrm{move}} = \sum_{k=\mathrm{M,S}} \int_{\Omega^{k,\mathrm{int}}} \nu \boldsymbol{B}_{\mathrm{PM}} \nabla \times \boldsymbol{R}_m^k d\Omega^k \tag{11}$$

$$L(\theta) = \int_{\Omega_{\mathrm{air}}} \nu \nabla \times F(R_m) \nabla \times F(R_m) T_m(\theta) \tag{12}$$

$$L_d(\theta) = \sum_{i=1}^{m-1} \int_{\Omega_{\mathrm{air}}} \nu \nabla \times F\left(R_i^k\right) \nabla \times F\left(R_m^k\right) T_i(\theta) \tag{13}$$

$$F(R) = \begin{cases} R^k, & \text{if node is not on slave interface} \\ \sum_j \kappa_j(\theta) R_j^k, & \text{if node is on slave interface} \end{cases} \tag{14}$$

$$H_{\mathrm{Lin}}(\theta) = \sum_{k=\mathrm{M,S}} \int_{\Omega^{k,\mathrm{int}}} \nabla \times R_i^k \nabla \times R_m^k d\Omega^{k,\mathrm{int}} T_i(\theta) \tag{15}$$

$$H_{\mathrm{NL}}(\theta) = \sum_{k=\mathrm{M,S}} \int_{\Omega^{k,\mathrm{int}}} \nabla \times (\boldsymbol{H}_{\mathrm{fp}}(\boldsymbol{A}_m(x,\theta)) \nabla \times \boldsymbol{R}_m d\Omega^k. \tag{16}$$

IV. Application to an Example Machine

In the following, the derived formulation is applied to a synchronous machine with surface-mounted magnets. The three-phase machine given in Fig. 2(a) has two pole pairs and a length of 12.5 cm. The permanent magnet remanence is set to 1.2 T. In Fig. 2(b), the airgap is depicted for a relative rotor angle of 22.5°. The absolute error tolerance for the ROM is set to 2×10^{-3}. The angular step is varied between 0° and 90° in 25 steps with a step width of 3.75°. The PGD is compared to reference solutions obtained on the same mesh with a standard magnetic vector potential solver.

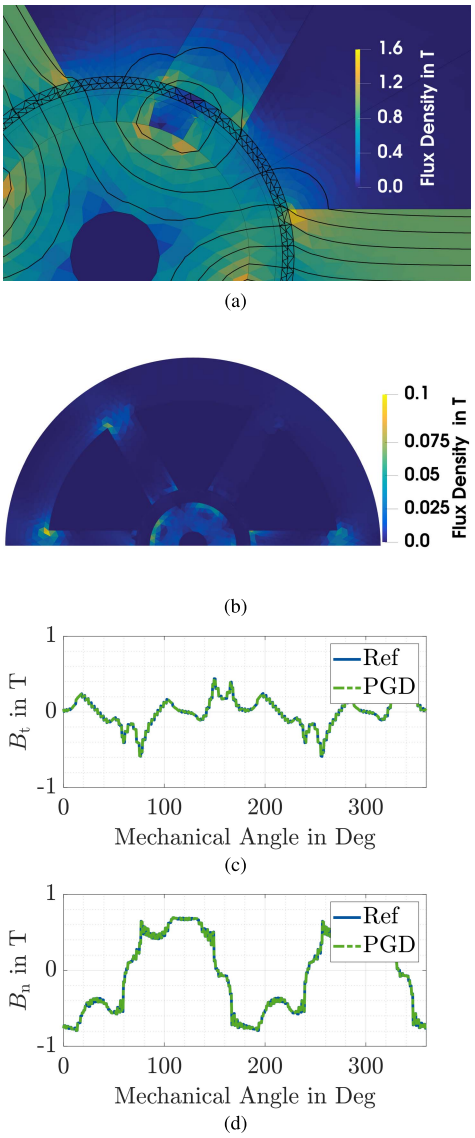

Fig. 3. Flux density for a rotor position of 22.5°. (a) Continuity of the magnetic vector potential lines at the interface. (b) $B_{\mathrm{ref}} - B_{\mathrm{PGD}}$. (c) Tangential airgap flux density. (d) Radial airgap flux density.

A. Airgap Fluxdensity

First, the continuity over the sliding interface is studied. In Fig. 3(a), the magnetic flux density and the equipotential lines of the magnetic potential are depicted for a rotational angle of 22.5°. It underlines that the ROM reproduces a physical solution. The difference of the reference's and ROM's flux densities in Fig. 3(b) shows the local error, which is mainly located in the rotor iron between the magnets and in the stator at the transition between tooth and yoke. Furthermore, to compute the torque of the machine or the forces acting on the ferromagnetic structure, the airgap flux density is derived and set in contrast to the reference solution. In Fig. 3(c) and (d), the tangential and radial flux densities in the middle airgap are shown. The results have very small deviations compared to the reference, which highlights the accuracy of the ROM.

B. Torque

In Section IV-A, the airgap flux density was studied in detail for one angular step, and in the following, the torque of the

Authorized licensed use limited to: Universitaetsbibliothek der RWTH Aachen. Downloaded on November 04,2022 at 11:31:00 UTC from IEEE Xplore. Restrictions apply.

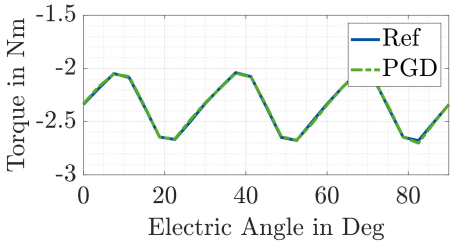

Fig. 4. Torque of the machine at $I_{\mathrm{dq}} = [0, -5]$ A and $B_{\mathrm{PM}} = 1.2$ T.

TABLE I
COMPUTATIONAL EFFORT OF DIFFERENT OPERATIONS

Method	Operation	Effort $O({N_x}^2)$
Standard FE	Build Matrix and Excitation	$N_{\mathrm{c}} \cdot N_\theta \cdot N_{\mathrm{NL}}$
Standard FE	Build Non-linear Load $\boldsymbol{H}_{\mathrm{fp}}$	$N_{\mathrm{c}} \cdot N_\theta \cdot N_{\mathrm{NL}}$
PGD	Solve Space Mode	$m \cdot N_{\mathrm{NL,PGD}}$
PGD	Solve Parameters Mode	$N_p \cdot m^2 \cdot N_{\mathrm{NL,PGD}}$
PGD	Build Non-linear Load $\boldsymbol{H}_{\mathrm{fp}}$	$m \cdot N_{\mathrm{c}} \cdot N_\theta \cdot N_{\mathrm{NL,PGD}}$

machine is depicted in Fig. 4. The overall torque characteristic is accurately approximated. Only in a few steps, small errors are identifiable.

C. Computational Effort

The combination of the PGD with the sliding interface technique pursues two objectives; on the one hand, the restriction to conformal meshes should be lifted; on the other hand, the computational effort compared to standard finite element computations should be reduced. The results regarding the continuity and reasonability of the approach are shown in Sections IV-A and IV-B. The computational effort of the reference computation and the worst case approximation of the enrichment process of the PGD are given in Table I. The parameter N_x denotes the DOF of the finite element (FE) model and N_c denotes the number of parameter combinations to be studied, excluding the number of angular steps, which is given by N_θ. N_{NL} is the number of non-linear iterations, which is not equal for the reference and the PGD. While the reference computation has to solve a non-linear finite element model for each step and each parameter combination, the PGD enrichment itself consists of an FE problem for computing the space mode and linear equations to compute the parameter modes. In the parameter computation, integrations over the mesh have to be performed to calculate the coefficients. The integration itself scales with N_x^2 and is conducted m times to compute a new mode m. Furthermore, if non-linear materials have to be considered, an additional load vector H_{fp} has to be built. Comparing the number of non-linear evaluations shows that the reference has a lower computational effort for non-linear simulations if N_{NL} is smaller than $N_{\mathrm{NL,PGD}} \cdot m$. By employing the DEIM, which only utilizes a small subset of elements and a projection operator, this effort is crucially reduced in the PGD to allow a faster evaluation of the non-linear term [9]. The number of modes to achieve a prescribed accuracy and the number of non-linear iterations to achieve a new mode are not known *a priori* and are problem-dependent. The effort of the online stage, which evaluates the magnetic vector potential $\boldsymbol{A}$ (4), is compared to the enrichment process almost negligible because it holds the sum over vectors multiplied by a scalar value, which scales with an effort of $O(N_x)$.

V. CONCLUSION

In this contribution, the PGD is combined with the sliding interface technique to include rotational motion and lift the limitation to conformal meshes without creating additional elements. By employing biorthogonal form functions, the resulting system of equations is symmetric positive semidefinite. The results highlight that the ROM can be used to study a rotating electrical machine with technical relevant accuracy, and a physical continuity at the interface is given. It can be summarized that the presented method is a reasonable tool; however, the reduction in terms of computational effort is strongly related to the application and the involved number of parameter combinations. The findings show that the PGD is extendable to non-separable problems by including additional curvature integrals, and it is conceivable that other methods to model motion are compatible with the PGD as well.

ACKNOWLEDGMENT

This work was supported by the German Research Foundation (DFG) (Numerical analysis of electromagnetic fields by proper generalized decomposition in electrical machines) under Research Project 347941356.

REFERENCES

[1] I. A. Tsukerman, "Overlapping finite elements for problems with motion," *IEEE Trans. Magn.*, vol. 28, no. 5, pp. 2247–2249, Sep. 1992.
[2] H. De Gersem, J. Gyselinck, P. Dular, K. Hameyer, and T. Weiland, "Comparison of sliding-surface and moving-band techniques in frequency-domain finite-element models of rotating machines," *COMPEL Int. J. Comput. Math. Electr. Electron. Eng.*, vol. 23, no. 4, pp. 1006–1014, Dec. 2004.
[3] O. J. Antunes *et al.*, "Using hierarchic interpolation with mortar element method for electrical machines analysis," *IEEE Trans. Magn.*, vol. 41, no. 5, pp. 1472–1475, May 2005.
[4] A. Christophe, L. Santandrea, F. Rapetti, G. Krebs, and Y. L. Bihan, "An overlapping nonmatching grid mortar element method for Maxwell's equations," *IEEE Trans. Magn.*, vol. 50, no. 2, pp. 409–4012, Feb. 2014.
[5] E. Lange, F. Henrotte, and K. Hameyer, "A variational formulation for nonconforming sliding interfaces in finite element analysis of electric machines," *IEEE Trans. Magn.*, vol. 46, no. 8, pp. 2755–2758, Aug. 2010.
[6] F. Müller, L. Crampen, T. Henneron, S. Clénet, and K. Hameyer, "Model order reduction techniques applied to magnetodynamic T-Ω-formulation," *COMPEL*, vol. 39, no. 5, pp. 1057–1069, 2020.
[7] L. Montier, T. Henneron, S. Clenet, and B. Goursaud, "Proper generalized decomposition applied on a rotating electrical machine," *IEEE Trans. Magn.*, vol. 54, no. 3, pp. 1–4, Mar. 2018.
[8] F. Müller, T. Henneron, S. Clenet, and K. Hameyer, "Error estimators for proper generalized decomposition in time-dependent electromagnetic field problems," *IEEE Trans. Magn.*, vol. 56, no. 1, pp. 1–4, Jan. 2020.
[9] T. Henneron and S. Clenet, "Application of the PGD and DEIM to solve a 3-D non-linear magnetostatic problem coupled with the circuit equations," *IEEE Trans. Magn.*, vol. 52, no. 3, pp. 1–4, Mar. 2016.
[10] B. P. Lamichhane, "Higher order mortar finite elements with dual Lagrange multiplier spaces and applications," Ph.D. dissertation, Universität Stuttgart, Stuttgart, Germany, 2006.
[11] B. I. Wohlmuth, "A comparison of dual Lagrange multiplier spaces for mortar finite element discretizations," *ESAIM: Math. Model. Numer. Anal.*, vol. 36, no. 6, pp. 995–1012, Nov. 2002.
[12] S. Chaturantabut and D. C. Sorensen, "Nonlinear model reduction via discrete empirical interpolation," *SIAM J. Sci. Comput.*, vol. 32, no. 5, pp. 2737–2764, 2010.

Authorized licensed use limited to: Universitaetsbibliothek der RWTH Aachen. Downloaded on November 04,2022 at 11:31:00 UTC from IEEE Xplore. Restrictions apply.